Changes in Structural and Electronic Properties of the Zeolite Framework Induced by Extraframework Al and La in H-USY and La(*x*)NaY: A ^{29}Si and ^{27}Al MAS NMR and ^{27}Al MQ MAS NMR Study

J. A. van Bokhoven, A. L. Roest, and D. C. Koningsberger*

Debye Institute, Department of Inorganic Chemistry and Catalysis, Utrecht University, Sorbonnelaan 16, 3508 TB Utrecht, The Netherlands

J. T. Miller

BP Amoco Research Center, E-1F, 150 West Warrenville Road, Naperville, Illinois 60563

G. H. Nachtegaal and A. P. M. Kentgens*

NWO/CW HF-NMR Facility, NSR Center, University of Nijmegen, Toernooiveld 1, 6525 ED Nijmegen, The Netherlands

Received: January 11, 2000; In Final Form: April 21, 2000

A ^{27}Al 3Q MAS, a quantitative ^{27}Al MAS, and a ^{29}Si MAS NMR study has been carried out on La(*x*)NaY and H-USY. Assignment of the different types of Al coordinations has been done using the results of the MQ MAS experiments. The ^{29}Si MAS and ^{27}Al MAS NMR results obtained at high fields (14.1 T) and fast MAS up to 27 kHz made a quantitative assignment possible of the framework and nonframework Al coordinations. It is shown that highly charged octahedrally coordinated extraframework Al causes a polarization inducing a quadrupolar broadening of part of the framework Al in ultrastable Y. A similar interaction is found for the framework of La(*x*)NaY due to the La^{3+} cations. In both cases, charged extraframework species polarize the framework Al. In La(*x*)NaY, La^{3+} in a cation position and in H-USY extraframework octahedral Al are the origin of the polarization. Besides this short-range polarization effect, an additional long-range effect is observed in La(*x*)NaY. This long-range geometrical effect causes an increase in both Si−O−Al and Si−O−Si angles depending on the La content.

I. Introduction

Ultrastable Y zeolite is a catalytically active compound, which is widely used in the fluid catalytic cracking process (FCC). To function as an active and stable catalyst, Y zeolite is stabilized by steaming. De-alumination of the zeolite takes place, creating extraframework aluminum (EFAl), which induces a stabilization of the framework. This process is accompanied by the creation of mesopores in the crystallites of the zeolite.[1] Moreover, for many reactions an increased catalytic activity is found.[2]

The activity of the Y zeolite in many reactions is a strong function of the steam activation treatment. An enhanced activity is observed after steaming, whereas more severe steaming causes a decrease in activity.[2] Much research has been carried out to understand this phenomenon, but no definite answers exist. It is well-known that type and number of acid sites strongly influence the activity of the catalyst.[3] The amount of EFAl species influences the cracking activity[4] significantly. In addition, the effect of mesopore formation is proposed to play a predominant role in the enhanced activity.[1]

Besides stabilization of a zeolite by steaming, incorporation of multivalent cations, like rare-earth elements, also increases the stability of the framework.[5] Moreover, it has been reported that incorporation of multivalent cations leads to an increase in the activity for e.g., *n*-hexane cracking.[6] Apparently, highly charged cations have a very similar effect on the activity as steaming but without the creation of mesopores. To be able to give more definite answers about the question of enhanced activity, a detailed knowledge of the structure is essential.

^{29}Si and ^{27}Al magic angle spinning (MAS) NMR has been widely applied to determine the structure of Y zeolites. ^{29}Si MAS NMR provides information about the Si/Al ratio of the framework, assuming Loewenstein's Rule[7] is obeyed. The isotropic chemical shift of aluminum in ^{27}Al MAS NMR provides information about the coordination of the aluminum species.[8] A complication of ^{27}Al MAS NMR is the second-order quadrupolar interaction of the central transition. As a result, resonances move from their isotropic chemical shift (δ_{CS}) due to the quadrupolar induced shift (δ_{QIS}) and broaden into specific powder line shapes, even under MAS conditions. Hence, the ^{27}Al MAS NMR spectra may consist of resonances shifted with respect to their isotropic chemical shifts, which are not well-resolved, and even some aluminum may escape detection due to extreme broadening. Therefore, care must be taken when interpreting ^{27}Al MAS NMR spectra. To obtain isotropic spectra, multiple quantum (MQ) MAS NMR[9,10] can be used. In a two-dimensional experiment, a correlation between the multiple and single quantum transitions is made, which leads to well-resolved spectra that have an isotropic dimension, free of any anisotropic quadrupolar broadening. This permits an unambiguous determination of the aluminum coordinations in the sample, and a simulation of the MQ MAS NMR spectra provides the NMR parameters and their distributions. These can then be used to

10.1021/jp000147c CCC: $19.00
Published on Web 07/01/2000

TABLE 1: Elemental Analysis (ICP)

sample	Na	La	Al	Si[b]
NaY	10.2[a]	0	11.3	30.3
La(3)NaY	8.6	3.1	11.4	29.5
La(6)NaY	7.5	6.1	11.3	28.7
La(11)NaY	5.0	11.2	10.9	27.8
La(17)NaY	4.2	16.7	10.3	25.8
H-USY	0.08	0	12.8	33.9
USYw	0.02	0	9.3	33.5

[a] All values are given in mass %. [b] Silicon is determined as the remainder.

simulate the ^{27}Al MAS NMR spectra, yielding quantitative information about the Al coordinations.

In this paper, we have applied (i) ^{29}Si MAS NMR to determine the Si/Al ratio of the zeolite framework and (ii) the multiple quantum ^{27}Al MQ MAS NMR technique (using the two-pulse/Z-filter scheme[11]) to study the different types of Al coordinations in La(*x*)NaY and H-USY zeolite. The use of a 600-MHz spectrometer and spinning speeds up to 27 kHz minimizes the chance that some aluminum escapes detection.[12] This is separately checked using a control sample. The framework structures and the Al coordinations of La(*x*)NaY and ultrastable Y are compared in detail.

II. Experimental Section

NaY is obtained commercially from Linde (LZ-Y54). The lanthanum-exchanged Y zeolites are obtained by exchanging NaY with $La(NO_3)_3$. Since $La(NO_3)_3$ (aq) is acidic, the lanthanum solution is added dropwise to a stirred slurry containing the zeolite. Lanthanum is quickly inserted in the zeolite, and the sodium is released. The pH was controlled to greater than 4 to avoid acid dealumination or sieve destruction. The exchange was carried out at room temperature. Upon calcination, the lanthanum ions exchange with the sodium in the sodalite cages. Samples are designated La(*x*)NaY, where *x* represents the weight percentage of lanthanum. This is done by choosing different concentrations of $La(NO_3)_3$ solution. The samples with 3.1, 6.1, and 11.2 wt % lanthanum were obtained after one $La(NO_3)_3$ exchange, which exchanges the sodium in the supercages. A sample with 16.7 wt % La [La(17)NaY] is obtained by a second exchange of the calcined La(11)NaY. For all of the catalysts, including NaY, a final sodium exchange is done to remove H^+ that is typically introduced during a lanthanum exchange. The exchanged zeolites were washed with demineralized hot water to remove excess salts before heating to 100 °C for drying. Finally, the zeolites were calcined by slowly heating to 300 °C at 1 °C/min and kept at the final temperature for 3 h. This allows the cations to migrate to the most stable coordination positions in the sodalite cages.

H-USY is a commercial catalyst, LZ-Y84. It is calcined at 450 °C using a heating rate of 1 °C/min and was kept at 450 °C for 4 h. A washed USY (USYw) was prepared by slurrying the H-USY with a 10% ammonium acetate solution for ~30 min. The pH was adjusted to 3 with sulfuric acid at 80 °C. The sample was filtered, washed three times with demineralized hot water, and dried at 120 °C for 24 h. Special attention was given to this sample to prevent dealumination through acid leaching during this treatment. Table 1 summarizes the contents of sodium, lanthanum, aluminum, and silicon in all samples as determined by elemental analysis using induced coupled plasma (ICP).

All samples were stored over a saturated NH_4Cl solution for at least 24 h before the NMR experiments were performed. After H-USY and USYw were measured by ^{27}Al MAS NMR, they were dried overnight at 220 °C, while they remained in the rotor and were subsequently remeasured. These samples are called H-USY(d) and USYw(d).

NMR Measurements. ^{29}Si MAS NMR measurements were performed on a Bruker AMX-500 spectrometer (B_0 = 11.7 T). Single pulse excitation spectra (SPE) were obtained at an MAS speed of ~5 kHz using a 90° pulse length of 7 μs. Chemical shifts, δ, are reported in ppm relative to tetramethylsilane. The relaxation delay was checked via saturation recovery. A relaxation delay of 60 s proved to be adequate for samples used in this study. For each spectrum, at least 100 scans were recorded to obtain a good signal-to-noise ratio. The spectra were deconvoluted and fitted with Gaussian curves to obtain the relative intensities of the peaks.

^{27}Al MAS NMR experiments were performed on a Bruker AMX-500 (B_0 = 11.7 T) and a Chemagnetics Infinity 600 (B_0 = 14.1 T). MAS was performed at a rotation speed of 14 and 27 kHz, respectively. The RF field strength was 31 and 36 kHz, respectively. To allow a quantitative evaluation of the spectra, excitation pulses of 0.7 μs were used, smaller or equal to the recommended $\pi/18$ pulse.[8] Chemical shifts, δ, are reported relative to aqueous $Al(NO_3)_3$. It was determined that relaxation delays of 0.5 s for the zeolitic samples were sufficiently long to permit quantitative analysis. Five hundred or 1000 scans were recorded for the ^{27}Al MAS NMR experiments. On the Bruker AMX-500, a home-built probe equipped with a Jakobsen 5-mm stator was used. In these experiments, silicon nitride rotors were employed that contain a small Al impurity which gives rise to a small signal at ~105 ppm. On the Chemagnetics Infinity 600, a Chemagnetics 2.5-mm X-H MAS probe was used.

^{27}Al 3Q MAS NMR experiments were carried out on a Bruker DMX-300, using a 2.5-mm BB-H MAS probe, and on a Chemagnetics Infinity 600 spectrometer, employing a 2.5-mm X-H MAS probe head. The 3Q excitation pulse was a π pulse, and the 3Q−1Q conversion pulse was a $\pi/3$ pulse. The RF field amounted to ~130 kHz on the DMX-300 and to ~170 kHz on the Infinity 600. The relaxation delay time was 0.5 s. MAS was performed at a rotation speed of 24 and 27 kHz, respectively. The MAS and MQ MAS spectra were simulated using a program developed in MATLAB taking distributions in NMR parameters into account.

To check if all aluminum is accounted for in the ^{27}Al MAS NMR spectra, the total intensities of the signal in the ^{27}Al MAS NMR spectra are compared to the intensity of samples with a known quantity of aluminum. Sample weights are corrected for water content by means of thermal gravitational analysis (TGA). Samples with well-known amounts of aluminum measured are α-Al_2O_3 ("Calcinet" from R&L Slaughter) and γ-Al_2O_3 (Condea, 230 m^2/g).

III. Results

A. ^{29}Si MAS NMR on La(*x*)NaY. Figure 1 displays the ^{29}Si MAS NMR spectra of the lanthanum-exchanged samples. At the bottom, the spectrum of NaY is given for comparison. The peaks in this spectrum are assigned as follows: $Q^4(n\text{Al})$ representing a Si atom bound to *n* −O−Al≡ groups and *4-n* −O−Si≡ groups. Each substitution of an −O−Si≡ by an −O−Al≡ brings about a deshielding effect of ca. 3 ppm. Neither for the NaY nor for the La(*x*)NaY samples is a Si atom with four −O−Al≡ [Q^4(4Al)] groups detected in the ^{29}Si MAS NMR spectra. It can be seen in Figure 1 that by increasing the lanthanum content to 17 wt %, the spectra gradually change. Peaks shift to higher field due to the presence of the 3-fold charged ion lanthanum.[13−16] Lanthanum cations are not mobile

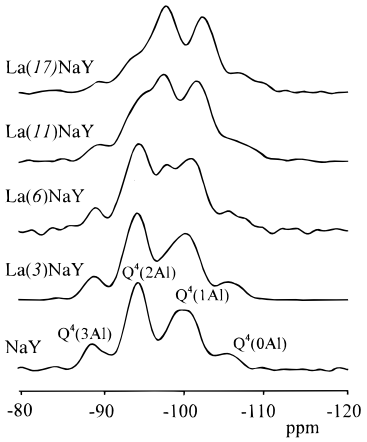

Figure 1. ^{29}Si MAS NMR of the La(*x*)Na Y samples, showing a gradual change in the spectra with increasing wt % lanthanum. Assignment of the peaks is given for NaY.

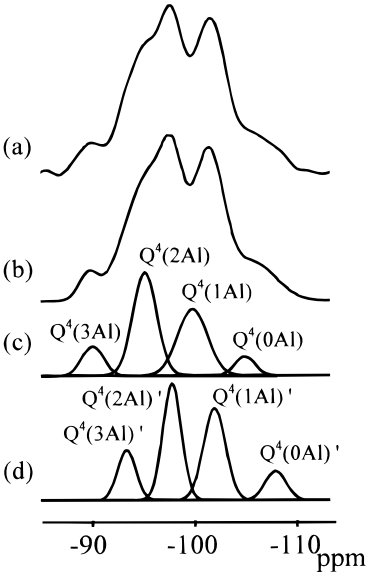

Figure 2. La(11)NaY is a typical example of a fitted ^{29}Si MAS NMR spectrum: (a) experimental spectrum; (b) total fitted spectrum; (c) four fitted peaks contributing to the NaY part, and (d) four fitted peaks contributing to the LaY part of the spectrum. In spectra c and d, the peak assignment is given.

in the pores of the zeolite due to the very strong electrostatic interaction of the lanthanum with the zeolitic framework.[17−20] Hence, only silicon atoms in the direct vicinity of the lanthanum ions will feel its presence and undergo a large shift. Therefore, the spectra of partly exchanged lanthanum can be built of two parts, namely, a fairly constant NaY part [with Q^4(nAl) peaks] and a fairly constant LaY part [with Q^4(nAl)′ peaks], in which all peaks are shifted to higher field as compared to the NaY spectrum. This is visualized in Figure 2 for the La(11)NaY sample. This figure gives a characteristic example of the results of the deconvolution procedure carried out on the spectra of the La(*x*)NaY samples. The experimental La(*x*)NaY spectra were fitted in several steps using the Bruker WinFit software.[21] First, the NaY part was obtained from the experimental NaY spectrum. In the first fitting step of La(*x*)NaY, only the overall intensity and the position of the complete NaY part was allowed to vary, whereas no restrictions were imposed on four additional Q^4(*n*Al)′ peaks, representing the LaY part of the spectrum. After a reasonable fit was obtained, the parameters of the four individual Q^4(*n*Al) peaks of the NaY part were included in the fitting procedure; first their intensities and then their positions and line width were released. So in the final refinement, all parameters of the eight lines were allowed to vary freely. For all La(*x*)NaY samples, a consistent fit was obtained using this procedure. In all cases, the LaY part was shifted approximately 3 ppm to high field (lower ppm values) with respect to the NaY part of the spectrum. On top of this, a gradual high field shift of all lines in the spectrum was observed with increasing La content of the samples. Table 2 summarizes the results of our deconvolution procedures. The estimated errors are given in brackets.

The intensities of the four peaks of each part can be used to calculate the overall Si/Al ratio of the framework. By applying Loewenstein's Rule,[7] which states that two tetrahedrally coordinated aluminum atoms on neighboring T positions are avoided, the following formula can be used:

$$\frac{\mathrm{Si}}{\mathrm{Al}} = \frac{\sum_{n=0}^{4} I_n}{\sum_{n=0}^{4} (n/4) I_n} \qquad (1)$$

where I_n is the intensity of the peak associated with Q^4(*n*Al). It can be seen in Table 2 that the Si/Al ratios in the La(*x*)NaY samples vary from 2.54 to 2.69. The noise level was chosen as the maximum deviation in intensity of the fitted peaks. The smallest peak used while fitting the spectra was about five times the noise level. Considering this error source, it can be concluded that no significant change in the Si/Al ratio occurs during La exchange.

Besides the large shift of 3 ppm to higher field of the LaY part, the overall spectrum shows a small gradual change in peak position to higher field with higher weight percentage of lanthanum. Figure 3 shows the gradual change in peak position of the peaks in the ^{29}Si MAS NMR spectra versus the lanthanum content of the zeolite. In the ^{27}Al MAS NMR spectra, a very similar shift in peak position is found (vide infra).

B. ^{27}Al MQ MAS NMR on La(*x*)NaY. MQ MAS NMR[9,10] is used to obtain isotropic spectra. The determination of isotropic chemical shifts makes an unambiguous assignment of the aluminum coordinations possible. Moreover, a simulation of the MQ MAS NMR spectra provides the NMR parameters and its distributions. The MQ MAS spectra are left unsheared so that the line $\nu_1 = 3\nu_2$, representing the isotropic chemical shift axis (where $\delta_{F2} = \delta_{F1}$) is plotted as the diagonal. Resonances that are positioned on this line correspond to Al that do not experience any or small quadrupolar coupling constants, C_{QCC}. A distribution in isotropic chemical shift is visible in the spectra by a broadening in the direction parallel to the diagonal. Al that experiences a large C_{QCC} corresponds to resonances that are deviating from the diagonal in the direction $\nu_1 = (3/4)\nu_2$ due to the quadrupolar-induced shift (δ_{QIS}). These lines are further broadened by the second-order quadrupolar interaction in the direction $\nu_1 = (19/12)\nu_2$. In Figure 5, the direction of the quadrupolar-induced shift (δ_{QIS}) and its anisotropic broadening are indicated. A broad distribution in quadrupolar interaction causes lines to bend away from the diagonal. The distributions in the MQ MAS spectra can be simulated, yielding the NMR parameters. However, as discussed extensively elsewhere,[10,11,22] the response of nuclei experiencing different quadrupolar interactions is nonuniform, leading to nonquantitative spectra. Moreover, the Gaussian distributions that are used to simulate the MQ MAS spectra do not have a physical interpretation. Nonetheless, good descriptions of the MQ MAS line shapes

TABLE 2: Deconvolution of the ^{29}Si MAS NMR Spectra of La(*x*)NaY

	NaY part				LaY part				Si/Al	Si/Al	Si/Al
sample	Q^4(3Al)	Q^4(2Al)	Q^4(1Al)	Q^4(0Al)	Q^4(3Al)′	Q^4(2Al)′	Q^4(1Al)′	Q^4(0Al)′	(NaY)	(LaY)	(total)
NaY	11	39	43	7					2.6 (<0.05)		2.58 (0.02)
La(3)NaY	10	37	38	7	2	2	3	2	2.6 (<0.05)	2.7 (0.3)	2.61 (0.05)
La(6)NaY	7	32	43	2	3	3	5	4	2.6 (<0.05)	3.0 (0.2)	2.69 (0.06)
La(11)NaY	7	21	23	4	7	13	19	6	2.5 (0.05)	2.7 (0.05)	2.61 (0.05)
La(17)NaY	4	14	10	3	7	30	28	5	2.5 (0.1)	2.6 (<0.05)	2.54 (0.04)

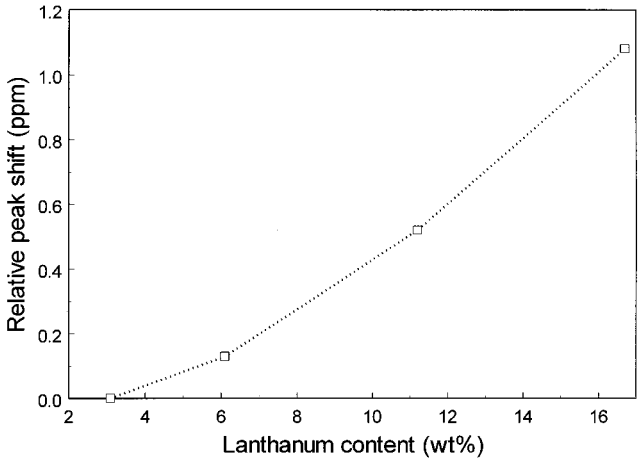

Figure 3. Shift in average peak position as a function of lanthanum content in the ^{29}Si MAS NMR. Peak positions are given relative to the corresponding peaks in the ^{29}Si MAS NMR spectra of La(3)NaY.

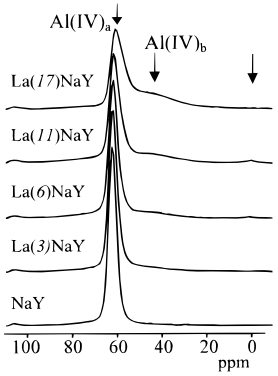

Figure 4. ^{27}Al MAS NMR spectra of the La(*x*)NaY samples, showing a gradual change in the spectra. While peak Al(IV)$_a$ decreases in intensity when more lanthanum is exchanged into the zeolite, peak Al(IV)$_b$ increases. An arrow at 0 ppm marks the position where octahedral Al would be visible in the spectra. Spectra are taken at B_0 = 11.7 T.

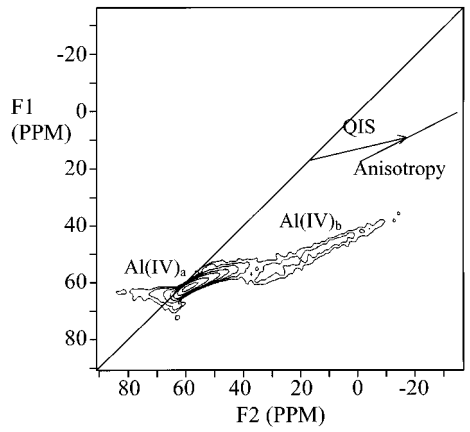

Figure 5. ^{27}Al 3Q MAS NMR spectrum of La(17)NaY. Peaks Al(IV)$_a$ and Al(IV)$_b$ have isotropic shifts of 61 and 60 ppm, respectively, indicating both correspond to tetrahedrally coordinated Al. Peak Al(IV)$_b$ shows a large quadrupolar interaction, due to the interaction with the trivalent charged lanthanum. Spectra are taken at B_0 = 7.1 T.

can be obtained, and the NMR parameters and their distributions are used to simulate the ^{27}Al MAS NMR spectra.[22] This procedure allows an unambiguous interpretation of the MAS spectra and a reliable quantification of the various Al species that are present.

Figure 4 shows the ^{27}Al MAS NMR spectra of the lanthanum-exchanged samples obtained at 11.7 T. The spectra of the samples containing lanthanum show a relatively narrow resonance at 61 ppm [peak Al(IV)$_a$] and a very broad resonance in the 40−50 ppm range [peak Al(IV)$_b$]. Clearly visible is a gradual increase of the broad peak Al(IV)$_b$ as the lanthanum content in the zeolite is increased. Peak Al(IV)$_a$ is visible in the NaY sample and all La(*x*)NaY samples and is attributed to tetrahedally coordinated aluminum in the zeolitic framework, which is charge-balanced by a sodium ion. None of the spectra show significant resonances around 0 ppm, which is the expected position for peaks corresponding to octahedral Al.

Peak Al(IV)$_b$ is assigned to distorted framework tetrahedral coordinated aluminum in correspondence with earlier reported results.[16,23] In ^{27}Al MAS NMR, several reasons for shifts in peak position exist. The peak position is a function of (i) the coordination number, (ii) the Al−O−Si angle, (iii) the mean Al−O distance, and (iv) the presence of quadrupolar interactions.[8] To obtain further information about the origin of peaks Al(IV)$_a$ and Al(IV)$_b$ in the La(*x*)NaY spectra, ^{27}Al MQ MAS NMR experiments are used. Figure 5 shows the ^{27}Al MQ MAS NMR of La(17)NaY, which is illustrative of all La(*x*)NaY samples with respect to peak shapes. (This spectrum is taken at B_0 = 7.1 T.) Peak Al(IV)$_a$ resonates close to the diagonal, indicating a very small quadrupolar interaction. The width of this peak is dominated by a distribution in isotropic shift, which can be due to a variation in bond angle. Peak Al(IV)$_b$ is shifted from the diagonal in the direction of the quadrupolar induced shift, indicated by an arrow (δ_{QIS}). The aluminum atoms represented by peak Al(IV)$_b$ experience a much larger quadrupolar interaction than the framework aluminum in peak Al(IV)$_a$. The NMR parameters are determined by a simulation of the peaks in the MQ MAS spectra. In all La(*x*)NaY samples, peaks Al(IV)$_a$ and Al(IV)$_b$ have approximately identical average isotropic chemical shifts (δ_{IS}). Hence both peaks can be assigned to tetrahedrally coordinated aluminum. The average quadrupolar couplings constants, C_{QCC}, of the peaks are 1.9 and 6.1 MHz, respectively. Therefore, the aluminums represented by peak Al(IV)$_a$ have a fairly symmetric surrounding, whereas the

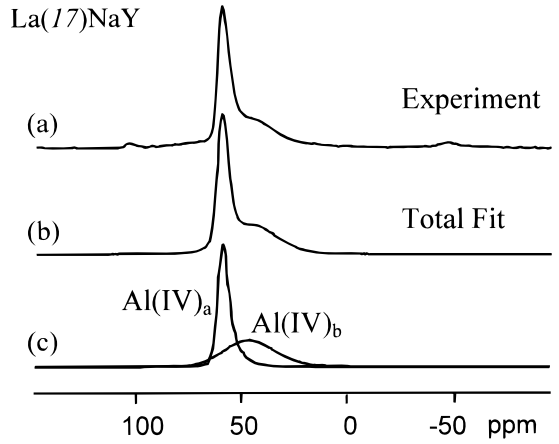

Figure 6. Deconvolution of the ^{27}Al MAS NMR spectrum of La(17)-NaY, using the NMR parameters and its distributions from simulations of the MQ MAS spectra: (a) experimental spectrum, b) fitted spectrum, and (c) deconvoluted peaks Al(IV)$_a$ and Al(IV)$_b$. Spectra are taken at $B_0 = 11.7$ T.

TABLE 3: Deconvolution of the ^{27}Al MAS NMR Spectra of La(*x*)NaY

	peak Al(IV)$_a$		peak Al(IV)$_b$	
sample	$<\delta_{IS}>$ (ppm)[a,c]	peak area (%)[d]	$<\delta_{IS}>$ (ppm)[b,c]	peak area (%)[d]
La(3)NaY	63.3	88	62	12
La(6)NaY	63.2	82	61	18
La(11)NaY	62.7	72	61	28
La(17)NaY	61.0	54	60	46

[a] $C_{QCC} = 1.9$ MHz. [b] $C_{QCC} = 6.1$ MHz. [c] ± 1 ppm. [d] $\pm 5\%$.

aluminum represented by peak Al(IV)$_b$ experiences a substantial electrical field gradient.

At 11.7 T, the quadrupolar interaction of peak Al(IV)$_b$ results in a position of the peak maximum at ~40 ppm. Figure 6 shows the deconvoluted ^{27}Al MAS NMR spectrum of La(17)NaY. A satisfactory simulation is obtained as the difference between the simulated and the experimental spectrum is within the level of noise. All other ^{27}Al MAS NMR spectra of La(*x*)NaY, as given in Figure 4, could be simulated using similar values for the averaged quadrupolar coupling constants, C_{QCC}, 1.9 and 6.1 MHz for peak Al(IV)$_a$ and Al(IV)$_b$, respectively. Best simulations were obtained when the isotropic shifts and their distribution were allowed to vary, using the δ_{IS} value for La(17)NaY as a starting point. Agreement within the noise level for all La(*x*)NaY samples is obtained. Quantitative results are presented in Table 3. The isotropic shifts of both peaks are given as well as their relative intensities. The average isotropic chemical shift of both peak Al(IV)$_a$ and peak Al(IV)$_b$ shows a small shift toward higher field with increasing La content. The shift of peak Al(IV)$_a$ can be distinctively seen in Figure 4. This shift is very similar to the shift in the ^{29}Si MAS NMR spectra shown in Figure 3. However, the ^{27}Al MAS NMR data should be interpreted with some caution, considering the large distributions in chemical shift and quadrupolar coupling constants used in the simulations.

C. ^{29}Si MAS NMR on Ultrastable Y. In Figure 7, the ^{29}Si MAS spectra obtained from H-USY and USYw are shown. The spectra look quite different from the La(*x*)NaY spectra as given in Figure 1: peaks with less $-$O$-$Al$\equiv$ neighbors now dominate the spectra. This directly indicates that aluminum has been removed from the framework during steaming. The spectra of H-USY and USYw are very similar. Using the assignments as given in Figure 7c, the spectra are deconvoluted and the total

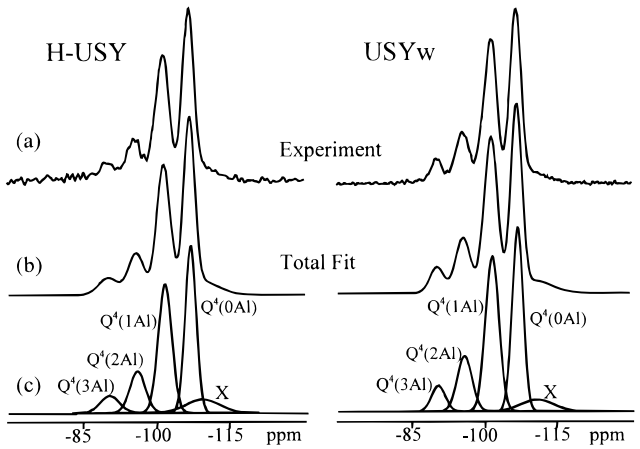

Figure 7. ^{29}Si MAS NMR spectra of H-USY and USYw: (a) experimental data, (b) total fitted spectrum, and (c) deconvoluted peaks with their assignment.

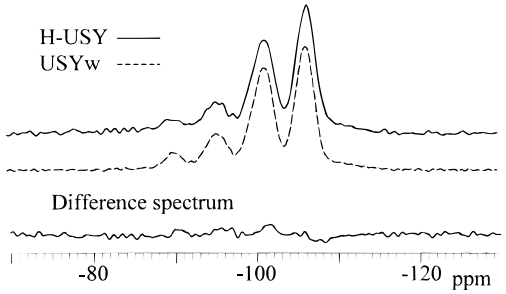

Figure 8. Difference ^{29}Si MAS NMR spectrum of H-USY and USYw, emphasizing that hardly any changes in the ^{29}Si MAS NMR spectra between H-USY and USYw exist.

TABLE 4: Aluminum Fractions from ICP and ^{29}Si NMR in Ultrastable Y

	NaY	H-USY	USYw
framework[a]	1	0.58	0.58
washed out[b]	0	0	0.28
extraframework	0	0.42	0.14

[a] Obtained from ^{29}Si NMR. [b] Obtained from ICP.

fit is shown in Figure 7b. While fitting, an additional peak at -110 ppm had to be added to reach a deconvolution within the noise level. This peak at -110 ppm (further denoted by X) is assigned to an amorphous silica phase.[24] Obeying Loewenstein's Rule and using eq 1, the Si/Al ratios for H-USY and USYw are determined to be 4.5 and 4.4, respectively. To further investigate the changes in the ^{29}Si MAS NMR spectra of H-USY and USYw, the spectrum of USYw is subtracted from the spectrum of H-USY in Figure 8. This shows that the difference between both spectra is very small.

D. ICP Experiments. Using ICP, the Si/Al ratio of the bulk is determined. The results of the ICP experiments indicate that 28% of all aluminum in H-USY is washed out after CH_3COONH_4 treatment (Table 1). By combining the results of ICP and ^{29}Si MAS NMR, it is now possible to calculate for NaY, H-USY, and USYw the amount of (i) framework aluminum, (ii) EFAl, and (iii) aluminum washed out of the pores of the zeolite (Table 4). Two-thirds of the EFAl is washed out with CH_3COONH_4, whereas one-third of the EFAl is still present in the pores. The removal of washable EFAl has a small effect on the ^{29}Si NMR spectrum (Figures 7 and 8). In USYw, ~19% [$= 0.14/(0.14 + 0.58) \times 100\%$] of the total aluminum is still left in pores of the zeolite as extraframework species, whereas ~81% is framework aluminum. On the basis of these numbers,

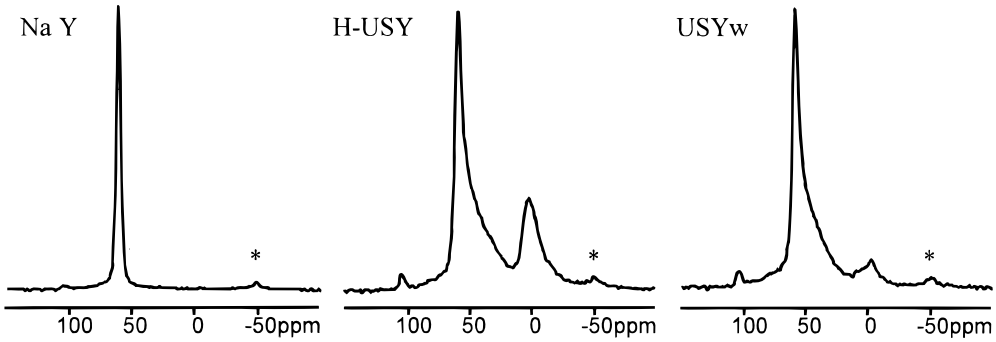

Figure 9. ^{27}Al MAS NMR spectra of NaY, H-USY, and USYw. All three spectra show a resonance at ~60 ppm [Al(IV)$_a$]. Both H-USY and USYw show a broad component at ~40 ppm (Al(IV)$_b$): the intensity at 0 ppm in USYw is largely diminished as compared to H-USY. Asterisk (*) denotes a spinning sideband. The intensity at ~105 ppm corresponds to Al in the rotor and is of no relevance to the samples. Spectra are taken at $B_0 = 11.7$ T.

a definite assignment of the peaks as visible in the ^{27}Al (MQ) MAS NMR can be made as to their position in or out the zeolite framework.

E. ^{27}Al (MQ) MAS NMR on Ultrastable Y. The ^{27}Al MAS NMR spectra of NaY, H-USY and USYw are given in Figure 9. These spectra show one resonance at ~60 ppm, which is already assigned to framework tetrahedral aluminum [comparable to peak Al(IV)$_a$ in the spectrum of La(*x*)NaY in Figure 4]. In addition, the spectra of H-USY and USYw show a broad component at ~40 ppm very similar to peak Al(IV)$_b$ in the spectra of La(*x*)NaY (Figure 4). In the NMR literature of H-USY, this broad component has been assigned to (i) distorted nonframework tetrahedral,[1,25−30] (ii) pentacoordinated aluminum species,[14,25−27] and (iii) tetrahedral framework aluminum.[29,31] The H-USY and USYw samples also show a peak at 0 ppm, which is in general attributed to extraframework octahedral aluminum or even to octahedral aluminum positioned in the framework.[32] The intensity of the 0 ppm peak in USYw is much lower than for H-USY. To be able to give a definite assignment to the peaks in the ^{27}Al MAS NMR spectra, the results of the simulation of the ^{27}Al MQ MAS NMR spectra have been used. To increase resolution, these experiments were performed at a magnetic field of 14.1 T and spinning speeds of up to 27 kHz. The NMR parameters that define the peak shapes are determined by a full simulation of the MAS and MQ MAS spectra similar to the procedure followed for La(*x*)NaY. Figure 10 shows the ^{27}Al MQ MAS NMR spectra of H-USY (panel A) and USYw (panel B). The MQ MAS plot of H-USY (Figure 10A) shows at least five contributions. Peak Al(IV)$_a$ resonates close to the diagonal ($\nu_1 = 3\nu_2$). The broad peak Al(IV)$_b$ present in Figure 9 at 40 ppm is now visible at ~55 ppm. Peak Al(IV)$_b$ is deviating from the diagonal, indicating a large quadrupolar interaction, which explains the shift from 40 to 55 ppm due to a smaller quadrupolar induced shift at the higher external magnetic field. The isotropic shift of peak Al(IV)$_b$ is ~60 ppm, proving this peak originates from tetrahedrally coordinated aluminum species. Two different types of octahedrally coordinated aluminum are present: peak Al(VI)$_a$ resonates on the diagonal, and peak Al(VI)$_b$ is quadrupolar broadened. Peak Al(V) slightly deviates from the diagonal and is assigned to five-coordinated aluminum. The intensity of peak Al(V) is less than one percent as compared to the intensities of the other peaks. In the ^{27}Al MQ MAS NMR spectrum of USYw (Figure 10B), peaks Al(VI)$_b$ and Al(V) can hardly be detected, showing that the corresponding aluminum species were washed out of the zeolite. The distorted octahedral aluminum [peak Al(VI)$_b$] disappeared from the spectrum, whereas the symmetric octahedral [peak Al(VI)$_a$] is unaltered. No other peaks appear in the spectrum, indicating that the washing with CH_3COONH_4 did not lead to the formation of new aluminum species.

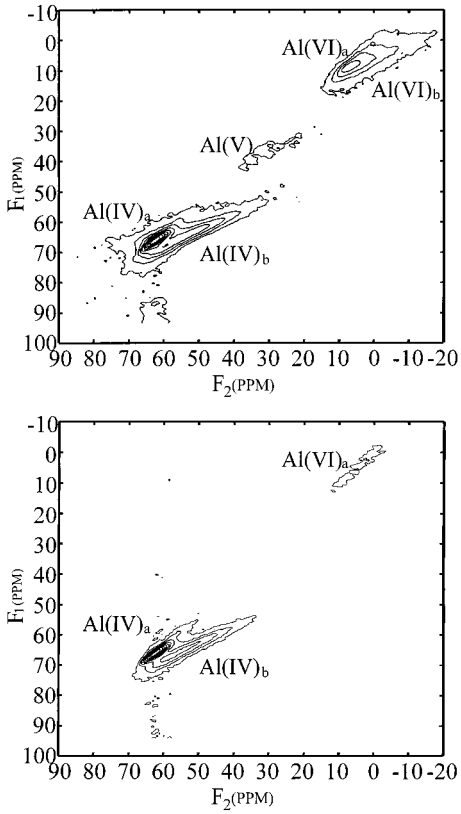

Figure 10. ^{27}Al MQ MAS spectra of (A) H-USY and (B) USYw. At least five contributions are visible in the spectrum of H-USY. In the spectrum of USYw, mainly peaks Al(V) and Al(VI)$_b$ have disappeared. Spectra are taken at $B_0 = 14.1$ T.

Figure 11 shows the ^{27}Al MQ MAS NMR spectra of the samples H−USY(d) (panel A) and USYw(d) (panel B). These samples were dried at 220 °C overnight, while they were staying in the rotors. The weight loss of the samples confirmed that water was largely removed. In the spectra of the dried samples, peak Al(IV)$_b$ is much more broadened than in the spectra of the corresponding wet samples. In the spectrum of H-USY(d), peak Al(V) is more pronounced visible than in the spectra of the wet H-USY sample, but it is almost absent in the spectrum of USYw(d). It is therefore assigned to nonframework aluminum, which can be washed out of the pores of the zeolite. This is also true for peak Al(VI)$_b$ in USYw(d). The octahedral aluminum corresponding to peak Al(VI)$_a$ is not washed out of the pores of the zeolite.

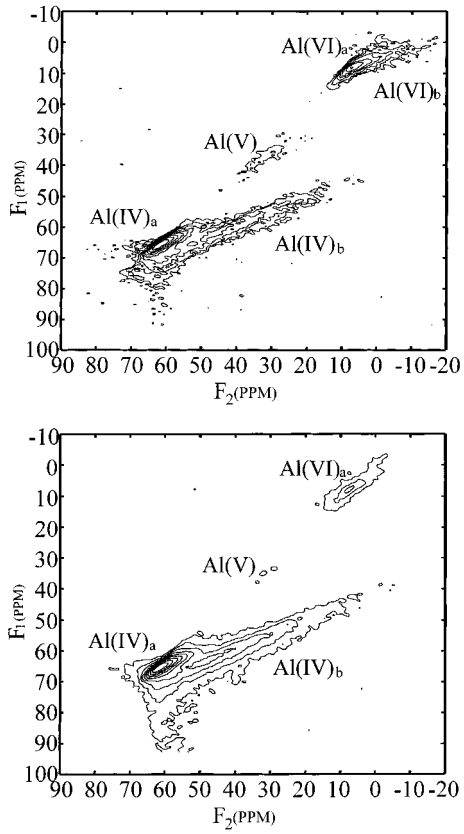

Figure 11. ^{27}Al MQ MAS spectra of (A) H-USY(d) and (B) USYw(d), showing an increased broadening of peak Al(IV)$_b$ in both spectra as compared to Figure 10. Peak Al(V) is now visible in both spectra. Spectra are taken at $B_0 = 14.1$ T.

TABLE 5: Peak Assignment in H-USY and USYw

assignment	$<\delta_{IS}>$ (ppm)[a]	$<C_{QCC}>$ (MHz)[b]	coord	frwk	H−USY[c]	USYw[c]
peak Al(IV)$_a$	62.8	2.2	tetrahedral	yes	0.36	0.33
peak Al(IV)$_b$	60.3	6.4	tetrahedral	yes	0.35	0.28
peak Al(VI)$_a$	8	3.0	octahedral	no	0.11	0.11
peak Al(VI)$_b$	8	5.0	octahedral	no	0.18	
peak Al(V)	35	4.4	5-coord	no	<0.01	
washed out	8	5.0	octahedral	no		0.28

[a] ±1 ppm. [b] ±0.5 MHz. [c] Values are given as fraction of total Al.

In general, drying samples can result in loss of intensity measured in the ^{27}Al MAS NMR, due to quadrupolar broadening of peaks. The integrated intensity of the NMR spectra of the H-USY sample was identical in wet and dry conditions within the error margin. The same is true for USYw. This proves that no peaks are broadened beyond detection. This indicates that at 14.1 T and spinning speeds of 27 kHz, no evidence for the presence of nonvisible aluminum in any of these samples exists. This is discussed in more detail in a later section.

The quadrupolar coupling constants, isotropic shifts, and their distributions were now determined by simulation of the MQ MAS spectra. The intensities of the peaks were obtained by simulating the ^{27}Al MAS NMR using the parameters as determined from the MQ MAS spectra. Table 5 summarizes the results from the ^{27}Al MAS and MQ MAS NMR simulations. Figure 12 gives the peaks used to deconvolute the experimental spectra. Figure 12b shows the results of the deconvolution procedure, which can be compared with the experimental ^{27}Al MAS NMR spectra in Figure 12a.

Subtracting the spectrum of USYw from H-USY gives the spectrum of the aluminum species washed out of H-USY. It

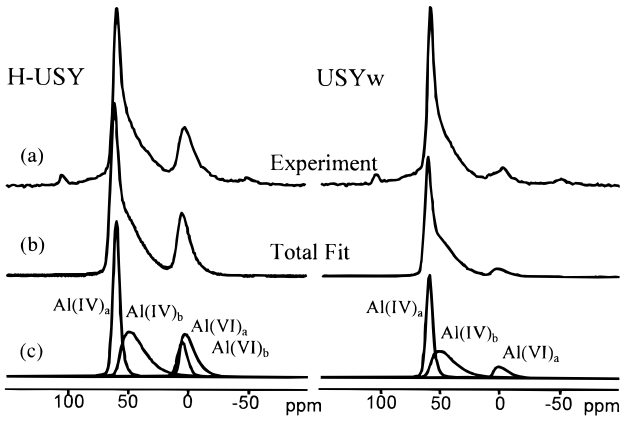

Figure 12. Deconvoluted ^{27}Al MAS NMR spectra of H-USY and USYw; (a) experimental data, (b) simulated spectra, and (c) deconvoluted peaks. Spectra are taken at $B_0 = 11.7$ T.

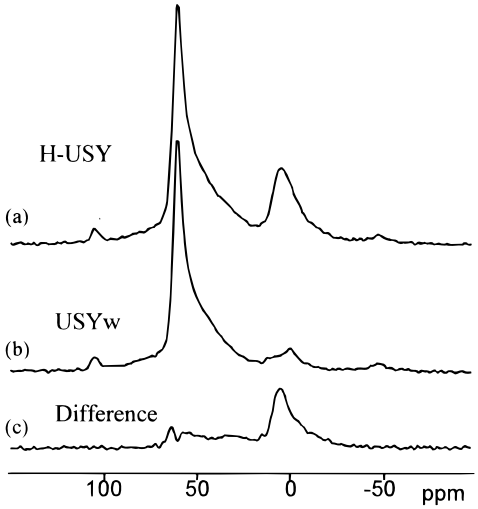

Figure 13. Difference ^{27}Al MAS NMR spectrum of H-USY and USYw, corresponding to the aluminum washed out of H-USY. Spectra are taken at $B_0 = 11.7$ T.

TABLE 6: Quantitative Analysis of ^{27}Al MAS NMR Spectra

sample	total intensity
α-Al_2O_3	1[a]
γ-Al_2O_3	1.01
NaY	1.03
H-USY	1.07
USYw	1.06

[a] Taken as a reference.

can be seen in Figure 13 that this difference spectrum consists mostly of octahedral aluminum [peak Al(VI)$_b$], whereas also in the region of 60 to 30 ppm intensity is visible.

IV. Discussion

A. Performing Quantitative ^{27}Al MAS NMR. The combination of ^{27}Al MAS with ^{27}Al MQ MAS NMR using a strong magnetic field of $B_0 = 14.1$ T and high spinning speeds allows for the quantitative determination of the aluminum coordinations in H-USY. Table 6 shows the intensity in the ^{27}Al MAS NMR spectra divided by the aluminum content in the samples obtained from ICP and TGA. The values given are relative to α-Al_2O_3. As shown in the literature,[33] the use of high spinning speeds (up to 29 kHz) can be necessary to account for all aluminum in aluminas. In Table 6, no systematic loss of intensity in the spectra of USY is found. All values coincide within the accuracy

of the integration method. Measurement of dried samples did not lead to any significant decrease in intensity in the spectra as compared to the wet samples. It can be concluded that no "NMR-invisible" aluminum is present in the USY samples and that all aluminum is accounted for in the ^{27}Al MAS NMR spectra.

B. Si/Al Ratio of La(*x*)NaY. In Table 2, the Si/Al ratios and the estimated errors for all La(*x*)NaY samples are given. Within the limits of accuracy, no evidence for any systematic variation in the Si/Al ratio in either the LaY or NaY part or in fact in the overall samples in the La(*x*)NaY samples can be found. It is concluded that the Si/Al ratio of each La(*x*)NaY sample is the same and equal to 2.6, the value of the parent NaY material. The fitting results are very similar to what has been reported[13−16] on comparable La(*x*)NaY samples. Gaare and Akporiaye[13] showed a systematic change in intensity of two constant parts as a function of lanthanum content of the zeolite. These parts were assigned to NaY and LaY, respectively, exactly as proposed here. Although their fitting procedure was somewhat different, they obtained a correlation between the relative intensities of both parts and the lanthanum content identical to results presented here.

Additional evidence for the lack of dealumination in the La(*x*)NaY samples is provided by the ^{27}Al MAS NMR. The ^{27}Al MAS NMR spectra of the La(*x*)NaY samples only show intensity in the 30−60 ppm range (Figure 4). No spectrum shows a resonance in the range of −20 to 20 ppm, which is the peak position of octahedral aluminum. Generally, the presence of octahedral aluminum indicates that dealumination of the framework has taken place. Combining this with the elemental analysis in Table 1, indicating no change in aluminum content in the samples, and the Si/Al ratios obtained from the ^{29}Si MAS NMR, it is concluded that all aluminum visible in ^{27}Al MAS NMR spectra of La(*x*)NaY is positioned in the zeolitic framework.

C. Framework Aluminum Coordinations in La(*x*)NaY. Table 3 summarizes the aluminum coordinations in La(*x*)NaY. The main difference between the samples is the enlarging area for peak Al(IV)$_b$ and the subsequent decrease of peak Al(IV)$_a$ upon increasing lanthanum content. This is expected when one assumes that all Al is framework Al of which Al(IV)$_b$ corresponds to Al experiencing a large quadrupolar interaction due to the presence of lanthanum.

Peak Al(IV)$_a$ and Al(IV)$_b$ are assigned to aluminum in the framework charge-balanced by a sodium and a lanthanum cation, respectively. The average quadrupolar couplings constants, C_{QCC}, of peaks Al(IV)$_a$ and Al(IV)$_b$ are 1.9 and 6.1 MHz. The ionic radius of sodium is 0.97 Å with a charge of +1, whereas the ionic radius of the lanthanum with charge 3+ is only a bit larger, i.e., 1.02 Å. Therefore, the Coulombic field around the lanthanum is much stronger than around the sodium ion. As a consequence, peak Al(IV)$_b$ experiences a much stronger electrical field gradient. This distorted electrical field can be induced by a geometrical distortion in the first coordination shell or to the presence of a charged ion, directly causing an electric field gradient. In a study of aluminosilicate glasses with a series of alkali ions as charge-balancing cations, a gradual increase in C_{QCC} with increasing polarization power of the alkali ions was observed.[34] A geometrically fixed structural model using point charges was able to reproduce the observed trend in increasing quadrupolar broadening on the aluminum: a smaller alkali atom is able to approach the aluminum closer, hence causing an increase in quadrupolar interaction. According to ab initio cluster calculations,[35] however, when protons are charge-balancing the negative zeolitic charge, it is the perturbation of the corresponding Al−O bonds that causes the quadrupolar distortion on the aluminum rather than electrostatic point charges or a geometric distortion in the O−Al−O angle. This is due to the large polarization power of the proton. Moreover, structural information obtained from XRD[17−20] indicate that small changes in T−O bond lengths occur when lanthanum is positioned on preferred cation positions in zeolite Y. The TO_4 tetrahedron, however, is hardly distorted.[36,37] On the basis of this, it is concluded that peak Al(IV)$_b$ is quadrupolar broadened by a combination of the two effects. The charged La^{3+} is directly inducing an electrical field gradient around part of the framework Al, and in combination with a small distortion of the Al−O bond lengths, a large quadrupolar interaction on this aluminum is found.

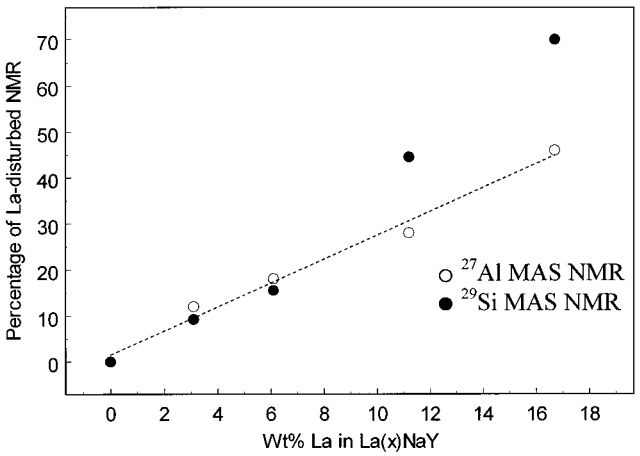

Figure 14. Contribution of peak Al(IV)$_b$ to the ^{27}Al MAS NMR spectra (○) and the LaY part in the ^{29}Si MAS NMR spectra (●) as a function of the lanthanum wt % in the La(*x*)NaY samples, showing a linear correlation of the intensity of La-disturbed Al with the amount of La in the zeolite.

Both peak Al(IV)$_a$ and Al(IV)$_b$ are broader when more lanthanum is exchanged into the zeolite, which is attributed to an increase in the distribution of bond angles. This can be understood when assuming that the charged lanthanum causes some strain on the zeolite framework, resulting in a larger spread in Al−O−Si angles.

From Table 3, it is clear that the intensity of peak Al(IV)$_b$ is a function of the weight percentage of lanthanum in the zeolite. Figure 14 establishes a linear relation between the relative intensity of peak Al(IV)$_b$ in the ^{27}Al MAS NMR spectra as a function of the weight percentage of lanthanum in the zeolite. This straight line indicates that, regardless the lanthanum loading, an identical fraction of the lanthanum exchanged into the zeolite is involved in charge-balancing the negative charges on the framework. Moreover, the spectra of all samples are best fitted using the same average quadrupolar coupling constant. As a consequence, it can be concluded that only one kind of lanthanum species is involved in charge-balancing the negative charge on the framework, irrespective of the loading of lanthanum in La(*x*)NaY. It can be seen that in the case of the ^{29}Si MAS NMR, the La-disturbed part in the spectra deviates from the linear line at the higher La loadings, indicating an increased disturbance of the silicon part of the framework as compared to the aluminum part.

On the basis of ^{29}Si MAS NMR data, Gaare and Akporiaye argued that the lanthanum-disturbed part of the framework in LaNaY samples correlates with the part of the zeolite whose charge is actually compensated by La^{3+} ions. Chao et al.[15] and

TABLE 7: XRD Results on La(*x*)NaY

sample	site I	site I′	site II	site II′	UC size (Å)	cationic charge[a]
NaY		16Na	26Na	15Na	24.66	57
La(3)NaY		1La + 20Na	26Na	2La + 2Na	24.67	58
La(6)NaY		4La + 13Na	27Na	2La	24.69	58
La(11)NaY		9La	28Na	2La	24.70	61
La(17)NaY	2La	14La	25Na	2La	24.73	79

[a] On the basis of a Si/Al ratio of 2.6, a cationic charge of 54 per unit cell is expected.

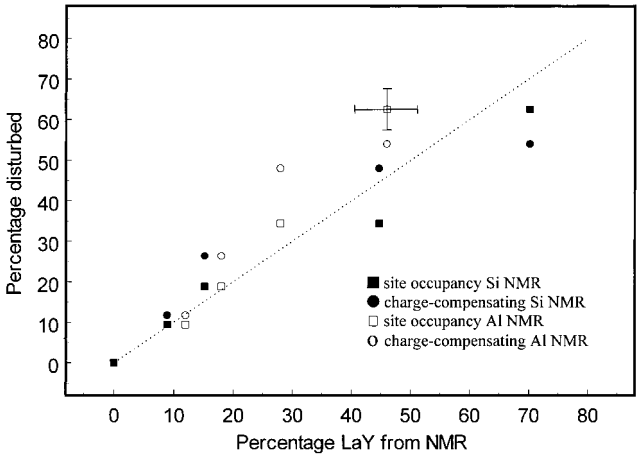

Figure 15. Correlation between the lanthanum-disturbed part of the zeolite as determined from ^{29}Si (solid symbols) and ^{27}Al NMR (open symbols) with the relative site occupancy model (squares) and the charge-compensating model (circles). See text for more details. Estimated maximum errors are given for one point.

Hunger et al.[16] argued that the disturbed part of the framework correlates with the relative occupancy of the SI′ site by lanthanum. The SI′ position is a preferred cation position in the sodalite cage, adjacent to a hexagonal ring. Other positions are the SII′ position, a site in the sodalite cage adjacent to an unshared hexagonal face, and the SI position, located in the center of a hexagonal prism. Thus, lanthanum ions located in SI′ and SII′ positions are always in the vicinity of six framework T atoms (either silicon or aluminum). Lanthanum on an SI position is affecting twelve T atoms. Using XRD, the relative occupancy of these sites, i.e., the part of the framework expected to be disturbed by lanthanum, can be determined. Table 7 gives the site occupancies as determined from XRD of the same samples[18] that are used to construct the amount of framework T sites disturbed by the lanthanum. A unit cell of zeolite Y contains 192 T positions, which result in a negative charge of 54 for a Si/Al ratio of 2.6. From Table 7, it is clear that an excess of cationic charge is present in the zeolite, assuming a charge of +3 for lanthanum. The disturbed part of the zeolite based on the charge-compensating model is independent of the site occupancy and can be calculated on the basis of the amount of lanthanum present on the lattice. This model assumes a constant cationic charge of 1 for sodium. Thus, the fraction of the spectrum that is expected to be influenced by sodium is calculated. The part of the zeolite disturbed by lanthanum is the remainder part of the spectrum. Hence, this model assumes all sodium present is charge-compensating the framework. Figure 15 shows the correlation between the distorted and undistorted part of the framework in the ^{29}Si MAS NMR spectra as determined using the relative site-occupation model (■) and the charge-compensating model (●). Considering the accuracy of the spectrum deconvolution and the refinement results of the XRD, both lines fulfill the ideal 1:1 dotted line, and no hard proof for any of the two models is obtained. It is therefore only concluded that the part of the framework that is disturbed correlates with the amount of lanthanum in the zeolite. Some modifications to the site-occupancy model lead to better agreement with the experiment (vide infra).

The same correlation between the Al disturbed by La [as visualized by the intensity of peak(IV)$_b$ in the ^{27}Al MAS NMR spectra] and the amount of La from the relative site occupancy model (□) and the charge-compensating model (○) can be made for the ^{27}Al NMR data as indicated in Figure 15. However, this does not lead to a preference for any of the two models either. Both models seem to overestimate the amount of interacting La in the pores of the zeolites as predicted from the ^{27}Al NMR data.

From Tables 1 and 7 it is clear that if all Na^+ and three-valent La^{3+} would be charge-balancing the framework, there is an excess of cationic charge. This is especially true for La(11)NaY and La(17)NaY. Moreover, a random distribution of Al over the framework of zeolite Y denotes that not all six rings contain an equal number of Al atoms. A Si/Al ratio of 2.6 implies on average 1.7 Al atoms in every six-ring. It may be expected that at low concentrations of lanthanum in the zeolite, at first the preferred ion positions in these six rings that bare the most negative charge will be occupied (i.e., with two or three Al atoms). As an example, placing charged lanthanum into a six-ring with two Al atoms will affect four Si atoms. Only at higher concentrations of lanthanum, sites in six rings with only one Al will be occupied, and five Si atoms per Al atom are disturbed. As a result, relatively more silicon atoms are disturbed at higher concentrations of lanthanum as compared to aluminum. The site-occupancy model as regarded in the previous section does not take into account the fact that the number of Al atoms in a six-ring is not constant. Therefore, assuming that at first the sites in six rings that have the most Al atoms are occupied, the site-occupancy model can be qualitatively improved. Looking at Figure 15, it can be seen that for low concentrations of La, the site-occupancy model predicts well the amount of distortion in both ^{27}Al and ^{29}Si MAS NMR, whereas, for higher La concentrations, the model overestimates the distortion in the ^{27}Al MAS NMR, whereas the distortion in the ^{29}Si MAS NMR is underestimated. Correcting for a preferred siting in six rings with more Al prior to six rings with only one Al atom, will result in a better agreement of the site-occupancy model with the experiment for both ^{27}Al and ^{29}Si MAS NMR. This corrected model agrees with the assumption that at higher loadings, lanthanum is exchanged as $La(OH)^{2+}$ species rather than as La^{3+}, since each cation is balancing less charge on the framework. This will be further investigated in a La NMR study.

D. Long-Range Effects in La(*x*)NaY. A shift to higher field in isotropic chemical shifts of all peaks in both ^{29}Si MAS NMR and ^{27}Al MAS NMR of the La(*x*)NaY samples is observed with increasing lanthanum content. This is indicated in Figure 3, which shows the additional isotropic shift of the average of the four peaks in the NaY and LaY part of the ^{29}Si MAS NMR spectra. The isotropic chemical shifts in ^{29}Si MAS NMR and ^{27}Al MAS NMR are a function of the Si−O−T[14] (T represents either Si or Al) and Al−O−Si angle,[38] respectively. Figure 3 indicates that on average the Si−O−T angles increase when more sodium is exchanged for lanthanum. The increase in angle is maximally ∼2°. The isotropic chemical shifts of the resonances in the ^{27}Al MAS NMR spectra on La(*x*)NaY as given in Table 3 show a very similar shift to lower δ with increasing lanthanum content. The large chemical shift quadrupolar

interaction distributions used in the simulations of peak $(IV)_b$ do not allow interpreting the observed small shift in detail, but the observed similar trend is remarkable.

The increase in Si−O−T and Al−O−Si angles indicates a long-range effect of the lanthanum on the zeolitic framework. The short-range effect was marked by a shift of ∼3 ppm in the ^{29}Si MAS NMR and a tripling of the quadrupolar coupling constant in the ^{27}Al NMR spectra. The zeolitic structure is adjusted in such a manner that it can accommodate the highly charged cations. Because of the covalent bonding in the zeolite,[39] this effect can extend over several bond lengths, and as a consequence, on average all T−O−T bond angles are increased, which is witnessed by an overall shift in both the Si and the Al chemical shifts as a function of La content. X-ray diffraction shows an increase in the unit cell volume with increasing amounts of lanthanum, which is in agreement with these findings.

E. Si/Al Ratio of Ultrastable Y Zeolite. The Si/Al ratio of the framework in ultrastable Y is determined from the ^{29}Si MAS NMR spectra using eq 1 (Figure 7), under the assumption that Loewenstein's Rule is obeyed. H-USY and USYw have a calculated Si/Al ratio of 4.5 and 4.4, respectively. This shows that very few changes have occurred to the framework after washing with 10% CH_3COONH_4.

It has been reported that nonzeolitic alumina silicate species present in the pores of zeolites may lead to erroneous conclusions about the Si/Al ratio of the framework.[40] On the basis of the small differences between the spectra of H-USY and USYw expressed in Figure 8, no indications of the presence of such species in H-USY exist. However, a small content of amorphous silica is present, visible as peak X at −110 ppm in the spectra of both H-USY and USYw. These species are assigned as nonframework but cannot be washed out of the pores of ultrastable Y. From this, it can be concluded that the washing procedure does not influence the framework of the USY: both samples have a very similar Si/Al ratio, and no acid leaching of the zeolite framework in H-USY has occurred.

F. Framework and Extraframework Al Coordinations in H-USY. In this section, the different types of Al coordinations in H-USY are discussed: (i) framework Al, (ii) extraframework Al, and (iii) Al washed out of the pores of the zeolites. This is done by combining the results of ICP (Table 1), ^{29}Si MAS NMR (Figures 7 and 8, Table 4), and ^{27}Al MAS NMR (Figures 9−12, Table 5).

On the basis of ICP and ^{29}Si MAS NMR, 58% of the aluminum present in H-USY is positioned in the framework, i.e., there is 42% nonframework Al. Washing removes 28% of all aluminum present in H-USY, without affecting the ^{29}Si MAS NMR spectra significantly (Figures 7 and 8). Apparently, this extraframework Al does not interact strongly with the framework, allowing them to be washed out with 10% CH_3COONH_4. In the ^{27}Al MAS NMR spectra, peak $Al(VI)_b$ and some intensity in the 60 to 30 ppm range has disappeared (Figure 13). This four-, five-, and six-coordinated Al is therefore assigned to EFAl (Table 5). Clearly, some amorphous Al_2O_3 species (compare, for example, the specra of amorphous alumina formed by sol−gel synthesis[41]) are removed from the zeolite. In USYw, 81% of all its aluminum is positioned in the framework, and 19% of the aluminum is still present as EFAl. (The values in Table 5 are normalized on the total amount of Al, the washed out Al inclusive.)

It has been proposed that zeolite Y may contain some octahedral aluminum associated with the framework, when the zeolite is in its acidic form.[32] After H-USY is washed, no evidence of transformation of octahedral to tetrahedral aluminum is found: no new tetrahedral species appear nor does any aluminum coordination increase in intensity in the NMR spectra. Only intensity is lost from the spectrum. Moreover, the reported amount of framework octahedral aluminum is rather small as compared to the amounts of octahedral aluminum in the ultrastable Y samples in this study. Hence, it is assumed that all octahedral aluminum in USYw is extraframework and, as a consequence, that also in H-USY [peaks $Al(VI)_a$ and $Al(VI)_b$] all octahedral Al is present as extraframework species. As a consequence, to account for the aluminum framework content, it must be concluded that peaks $Al(IV)_a$ and $Al(IV)_b$ in H-USY and USYw are connected to the framework (Table 5).

^{27}Al MQ MAS NMR (Figures 5 and 10) indicates that both La(*x*)NaY and H-USY contain a quadrupolar broadened resonance [peak $Al(IV)_b$]. In both samples, the corresponding aluminum is shown to be associated with the framework. In the La(*x*)NaY samples, La^{3+} is causing a large quadrupolar interaction as discussed in a previous section. The resemblance between peaks $Al(IV)_b$ in La(*x*)NaY and ultrastable Y suggests a similar origin in both type of samples.[31] Since in H-USY and USYw this quadrupolar peak $Al(IV)_b$ corresponds to a framework aluminum, it is concluded that the large quadrupolar interaction is induced by charged EFAl. The octahedral EFAl [peak $Al(VI)_a$] is proposed to be responsible for this interaction. The ratio of intensity of peak $Al(VI)_b$ to peak $Al(IV)_a$ is 0.39 (Table 5). Assuming a framework negative charge of −1 for every framework tetrahedral Al, the extraframework octahedral aluminum must bare on average a charge of +2.5. This shows that to charge-compensate the charge on the framework like the lanthanum in La(*x*)NaY, this EFAl must be highly dispersed over the zeolite. The presence of highly dispersed extraframework species has already been proposed.[1] This octahedral Al could not be washed out of the pores of the zeolite by 10% CH_3COONH_4. The mutual attraction of the highly charged extraframework octahedral aluminum and the negative charge on the framework of the zeolite prevents the EFAl from being washed out of the pores of the zeolite. To further investigate the interaction of the EFAl with the framework tetrahedral aluminum, the USY samples were dried and subsequently measured using ^{27}Al MQ MAS NMR. In Figures 10 and 11, it can be seen that drying the ultrastable Y zeolite causes peak $Al(IV)_b$ to broaden even further in the ^{27}Al MAS NMR spectra. Drying of the zeolite causes water to be removed from the pores of the zeolite, and hence, the charged extraframework octahedral aluminum can now approach the framework atoms more closely. As a result, the electrical field gradient increases and in addition, a local distortion in the Al−O bond lengths will occur due to an increased interaction. Both these effects increase the quadrupolar interaction of the octahedral Al [peak $Al(VI)_a$] with the framework tetrahedral Al [peak $Al(IV)_b$].

In both La(*x*)NaY and USY, the quadrupolar interaction of peak $Al(IV)_b$ is visible as a relatively narrow ridge (Figures 5, 10, and 11). A distribution in isotropic chemical shift is visible by broadening parallel to the diagonal. The narrow ridge indicates a small distribution in chemical shift on the distorted tetrahedral aluminum. All distorted tetrahedral aluminum experience a very similar interaction for both La(*x*)NaY and USY. Apparently, a specific interaction of the charge-compensating ions (La versus Al) with the tetrahedral framework is present. It is emphasized here that amorphous alumina species in general exhibit a broad isotropic chemical shift and quadrupolar interaction distribution, causing a specific shape of the resonances in the MQ MAS spectra, bending them away from the

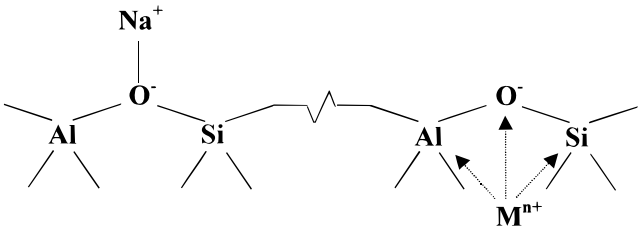

Figure 16. Model representing the framework of zeolite H-USY and La(*x*)NaY. Extraframework cations (M^{n+}), either La^{3+} or highly charged extraframework Al, are distorting the framework in La(*x*)NaY and H-USY, respectively.

diagonal. The distribution in isotropic chemical shift is comparable for both tetrahedral peaks in the samples in this study, which supports the idea that both tetrahedral Al [peaks $(IV)_a$ and $(IV)_b$] are positioned in the framework.

G. Identical Framework Structures of La(*x*)NaY and Ultrastable Y. The framework of both La(*x*)NaY and ultrastable Y zeolites can be represented by a simple structural model, which is shown in Figure 16. In both zeolites, part of the framework is distorted by a nonframework cation (M^{n+}). In ultrastable Y, the polarizing cation is a highly charged extraframework octahedral Al [peak $Al(VI)_a$], and in La(*x*)NaY it is a La^{3+} cation. In both cases, these cations are well-dispersed over the zeolite, causing a local distortion of the framework. This results in a quadrupolar broadened peak in the ^{27}Al MAS NMR spectra [peak $Al(IV)_b$].

The local distortion of the framework is accompanied by a long-range effect. The highly charged cations induce a distortion in the average T−O−T angle throughout the zeolite framework. In La(*x*)NaY zeolites, an increased lanthanum content resulted in larger average T−O−T angles.

H. Consequences for Catalysis. The Brønsted acidic catalytic active form of the zeolites are the protonic zeolites. Both H-USY and H(La)Y have an increased activity for catalytic cracking as compared to HY.[6,42] This similarity is accompanied by identical changes in both structures, as shown in this study. In H-USY, the formation of mesopores has occurred, which is not the case in La(*x*)NaY. A recent study on enhanced cracking activity[42] showed that a small increase in the external surface of the steamed Y zeolite already results in a large increase in catalytic activity. However, mesopore formation was found not to be able to account for the complete increase in activity, and it was suggested that sites of increased activity could be present in both H-USY and H(La)Y. It is possible that the interaction of the protons attached to the oxygens bridging the framework Si and Al atoms becomes weaker with increasing amounts of La in La(*x*)NaY or extraframework Al in H-USY due to the polarization induced by La^{3+} or Al^{3+}(EF). This will increase their Brønsted acid strength.[43]

It is known that the basicity on the framework of Y zeolites containing alkali cations as charge-compensating ions is a function of the electronegativity of the charge-compensating cations. The O(1s) and Al(1s) binding energies shift accordingly.[44−46] This has been explained by a decrease in Madelung potential of the corresponding zeolite.[46] An increase in polarization power of the ions present as charge-compensating species results in a progressive interaction with the tetrahedral framework aluminum. This becomes visible by an increased quadrupolar interaction. For lanthanum-exchanged zeolites, which have a much larger polarization power than any of the alkali ions, the larger effect is expected. This is also true for the extraframework Al^{3+} ion with a small ionic radius of 0.51 Å. In USY, it is the strong polarization power of this highly charged EFAl that is causing an effect identical to the lanthanum in La(*x*)-NaY. The Madelung potential for these two zeolites is expected to be decreased even further than in the alkali-exchanged zeolites. As a consequence, the oxygen atoms in the La(*x*)NaY and the USY are less basic than in NaY or any other alkali ion-exchanged zeolite.

The highly charged nonframework species distort the framework, causing a local distortion. A direct polarization or geometrically distortion on an approximate acid site may enhance the activity of this acid site.[6] In addition, a long-range effect induces a change in Si−O−T angle, which also influences acidity.[47] These subtle changes in the structure may also have an influence on the absorption capacity of the zeolites, which as a consequence, will influence catalytic activity. Whatever the exact cause of the increased catalytic activity, the paralleled framework distortions and changes in catalytic activity for both zeolites are striking and strongly suggest an identical cause of any increased activity, besides the mesopore formation in H-USY. On the basis of structural properties, H(La)Y can thus be used as a reference compound for H-USY.

V. Conclusions

Combining ^{27}Al MAS NMR with ^{27}Al MQ MAS NMR and ^{29}Si MAS NMR, a quantitative assignment of Al framework and extraframework coordinations in H-USY could be made. Well-dispersed and highly charged extraframework octahedral Al is producing an interaction with the framework. As a consequence, a quadrupolar broadened (framework) tetrahedral peak in the ^{27}Al MAS NMR spectrum becomes visible. This peak is also visible in ^{27}Al MAS NMR spectra of La(*x*)NaY. Here, the quadrupolar broadened tetrahedral Al peak is attributed to a framework tetrahedral Al interacting with La^{3+}. By comparing the NMR data of La(*x*)NaY to those of H-USY, it is concluded that the framework structures of zeolites La(*x*)NaY and USY are distorted similarly: both framework structures experience the interaction of well-dispersed charged extraframework cations. Moreover, the charged extraframework cations cause a long-range effect: a gradual increase in average Si−O−Al and Si−O−Si angles is observed when more charged extraframework cations are present in the pores of the zeolite. The comparable framework structures of La(*x*)NaY and H-USY, besides an increased mesopore volume for USY, strongly suggest an identical origin of the enhanced catalytic activity found for the active form of both zeolites for (acid-catalyzed) reactions.

References and Notes

(1) Beyerlein, R. A.; Choi-Feng, C.; Hall, J. B.; Huggins, B. J.; Ray, G. J. *Top. Catal.* **1997**, *4*, 27.

(2) Haag, W. O. *Studies in Surface Science and Catalysis*; Weitkamp, J., Karge, H. G., Pfeifer, H., Hölderich, W., Eds.; Elsevier Science BV: New York, 1994; Vol. 84, p 1375.

(3) Klyachoko, A. L.; Kapustin, G. I.; Brueva, T. R.; Rubinstein, A. M. *Zeolites* **1987**, *7*, 119.

(4) Lago, R. M.; Haag, W. O.; Mikovski, R. J.; Olson, D. H.; Bellring, S. D.; Schmitt, K. D.; Kerr, G. T. *New Dev. Zeolite Sci. Technol.* **1986**, *28*, 677.

(5) (a) Venuto, B. P.; Habib, T. E., Jr. *Fluid Catalytic Cracking with Zeolite Catalysts*; Marcel Dekker: New York, 1979. (b) Costenoble, M. L.; Mortier, W. J.; Uytterhoeven, J. B. *J. Chem. Soc., Faraday Trans. 1* **1977**, *73*, 466. (c) Rabo, J. A.; Angell, C. L.; Schomaker, V. In *Proceedings of the 4th International Congress on Catalysis*; Moscow, 1968; Elsevier: Amsterdam, Prep. 54.

(6) Carvajal, R.; Chu, P.; Lunsford, J. H. *J. Catal.* **1990**, *125*, 123.

(7) Loewenstein, W. *Am. Mineral.* **1954**, *39*, 92.

(8) Kentgens, A. P. M. *Geoderma* **1997**, *80*, 271.

(9) Frydman, L.; Harwood, J. S. *J. Am. Chem. Soc.* **1995**, *117*, 5367.

(10) Medek, A.; Harwood, J. S.; Frydman, L. *J. Am. Chem. Soc.* **1995**, *117*, 12779.

(11) Amoureux, J. P.; Fernandez, C.; Steuernagel, S. *J. Magn. Reson., Ser A.* **1996**, *123*, 116.
(12) Kraus, H.; Prins, R.; Kentgens, A. P. M. *J. Phys. Chem.* **1996**, *100*, 16336.
(13) Gaare, K.; Akporiaye, D. *J. Phys. Chem. B* **1997**, *101*, 48.
(14) Engelhardt, G.; Michel, D. *High-Resolution Solid-State NMR of Silicates and Zeolites*; Wiley: New York, 1987; Chapter V.3.4.
(15) Chao, K. J.; Chern, J. Y.; Chen, S. H.; Shy, D. S. *J. Chem. Soc., Faraday Trans.* **1990**, *86*, 3167.
(16) Hunger, M.; Engelhardt, G.; Weitkamp, J. *Microporous Mater.* **1995**, *3*, 497.
(17) Shy, D. S.; Chen, S. H.; Lievens, J.; Liu, S. B.; Chao, K. J. *J. Chem. Soc., Faraday Trans.* **1991**, *87*(17), 2855.
(18) Kaduk, J. A.; Faber, J. *Rigaku J.* **1995**, *12*(2), 14.
(19) Lee, E. F. T.; Rees, L. V. C. *Zeolites* **1987**, *7*, 143.
(20) Klein, H; Fuess, H. *J. Chem. Soc., Faraday Trans.* **1995**, *91*(12), 1813.
(21) Massiot, D. *Bruker WinFit*, version 930501; CNRS-CRPHT.
(22) Iuga, D.; Simon, S.; De Boer, E.; Kentgens, A. P. M. *J. Phys. Chem. B.* **1999**, *103*, 7591.
(23) van Bokhoven, J. A.; Roest, A. L.; Kentgens, A. P. M.; Koningsberger, D. C. In *Proceedings of the 12th International Zeolite Conference*; Treacy, M. M. J., Marcus, B. K., Bisher, M. E., Higgins, J. B., Eds.; MRS: Waarendale, PA, 1999; p 2515.
(24) Derouane, E. G.; Nagy, J. B. In *Relationship between Structure and Activity*; Whyte, T. E., Jr., Dalla Betta, R. A., Derouane, E. G., Baker, R. T. K., Eds.; ACS Symposium Series 248; American Chemical Society: Washington, DC, 1984; p 101.
(25) Rocha, J.; Klinowski, J. *J. Chem. Soc., Chem. Commun.* **1991**, 1121.
(26) Yang, X.; Truitt, R. E. *Zeolites* **1996**, *16*, 249.
(27) Yang, X. *J. Phys. Chem.* **1995**, *99*, 1276.
(28) Peters, A. W.; Wu, C. C. *Catal. Lett.* **1995**, *30*, 171.
(29) Freude, D.; Brunner, E.; Pfeifer, H.; Prager, D.; Jerschkewitz, H.-G.; Lohse, U.; Oehlmann, G. *Chem. Phys. Lett.* **1987**, *139*(3, 4), 325.
(30) Kellberg, L.; Linsten, M.; Jakobsen, H. J. *Chem. Phys. Lett.* **1991**, *182*, 120.
(31) Koningsberger, D. C.; Miller, J. T. *Studies in Surface Science and Catalysis*; Elsevier Science BV: New York, 1996; Vol. 101, p 841.
(32) Wouters, B. H.; Chen, T.-H.; Grobet, P. J. *J. Am. Chem. Soc.* **1998**, *120*, 11419.
(33) Kraus, H.; Müller, M.; Prins, R.; Kentgens, A. P. M. *J. Phys. Chem. B* **1998**, *102*, 3862.
(34) Dirken, P. J.; Nachtegaal, G. H.; Kentgens, A. P. M. *Solid State Nucl. Magn. Reson.* **1995**, *5*, 189.
(35) Koller, H.; Meijer, E. L.; van Santen, R. A. *Solid State Nucl. Magn. Reson.* **1997**, *9*, 165.
(36) Navrotski, A.; Geikinger, K. L.; McMillan, P.; Gibbs, G. V. *Phys. Chem. Miner.* **1995**, *11*, 284.
(37) Kubicki, J. D.; Sykes, D. *Phys. Chem. Miner.* **1993**, *19*, 381.
(38) Lippmaa, E.; Samoson, A.; Mägi, M. *J. Am. Chem. Soc.* **1986**, *108*, 1730.
(39) van Santen, R. A.; Kramer, G. J. *Chem. Rev.* **1995**, *95*, 637.
(40) Lutz, W.; Wieker, W.; Müller, D.; Schneider, M.; Rüscher, C. M.; Buhl, J.-Ch. *Z. Anorg. Allg. Chem.* **2000**, *626* (6), 1460.
(41) Simon, S.; van Moorsel, G. J.; Kentgens, A. P. M.; de Boer, E. *Solid State Nucl. Magn. Reson.* **1995**, *5*, 163.
(42) Williams, B. A.; Babitz, S. M.; Miller, J. T.; Snurr, R. Q.; Kung, H. H. *Appl. Catal., A* **1999**, *177*, 161.
(43) Carvajal, R.; Chu, P.-J.; Lunsford, J. *J. Catal.* **1990**, 125, 123.
(44) Okamoto, Y.; Ogawa, M.; Maezawa, A.; Imaka, T. *J. Catal.* **1988**, *112*, 427.
(45) Stoch, J.; Lercher, J.; Ceckeiwicz, S. *Zeolites* **1992**, *12*, 82.
(46) Grünert, W.; Muhler, M.; Schröder, K.-P.; Sauer, J.; Schlögel, R. *J. Phys. Chem.* **1994**, *98*, 10920.
(47) Carson, R.; Cooke, E. M.; Dwyer, J.; Hinchliffe, A.; O'Malley, P. J. In *Zeolites as Catalysts Sorbents and Detergent Builders, Extended Abstracts* 1988; Elsevier: Amsterdam; p 151.